Applied Catalysis B: Environmental 174–175 (2015) 203–211

Contents lists available at ScienceDirect

Applied Catalysis B: Environmental

journal homepage: www.elsevier.com/locate/apcatb

Electrocatalytic activity of Vulcan-XC-72 supported Pd, Rh and Pd_xRh_y toward HOR and ORR

F. Tzorbatzoglou [a], A. Brouzgou [a], P. Tsiakaras [a,b,*]

[a] Department of Mechanical Engineering, School of Engineering, University of Thessaly, Pedion Areos, 38334 Volos, Greece
[b] Laboratory of Electrochemical Devices based on Solid Oxide Proton Electrolytes, Institute of High Temperature Electrochemistry, 620990 Yekaterinburg, Russia

ARTICLE INFO

Article history:
Received 12 November 2014
Received in revised form 7 February 2015
Accepted 2 March 2015
Available online 5 March 2015

Keywords:
Hydrogen oxidation reaction
Oxygen reduction reaction
Palladium
Rhodium
Non-platinum catalysis

ABSTRACT

Carbon-supported (Vulcan XC-72) Pd, Rh, and Pd_xRh_y (20 wt%, x:y = 1:1, 3:1, 1:3) electrocatalysts are prepared according a modified pulse-microwave assisted polyol synthesis method and their electrocatalytic activity toward hydrogen electrooxidation (HOR) and oxygen reduction (ORR) reactions is investigated.

The as-prepared electrocatalysts are physicochemically characterized by transmission electron microscopy (TEM) and X-ray diffraction (XRD). Their electrochemical characterization is carried out by the aid of cyclic voltammetry (CV), rotating disk electrode (RDE) and chronoamperometry (CA) techniques.

It is found that among the as-prepared catalysts, $PdRh_3$ exhibits the highest HOR (i_k = 7.6 mA cm^{-2}) and ORR (i_k = 5.20 mA cm^{-2}) electrocatalytic activity. It is also found that the addition even of small amount of Rh (Pd_3Rh-2.7 μg cm^{-2}) enhances both Pd's HOR and ORR electrocatalytic activity by 33% and by 53%, respectively.

For the as prepared electrocatalysts, the HOR activity order, in terms of kinetic current density, is found to be as follows: $PdRh_3 \approx PdRh > Rh > Pd_3Rh > Pd$, while a similar trend was found for ORR activity: $PdRh_3 > PdRh > Rh > Pd_3Rh > Pd$.

1. Introduction

Platinum based electrocatalysts, due to its excellent catalytic activity, still remains the most commonly used for both the hydrogen oxidation and oxygen reduction reactions. However, the high cost and the limited resources of platinum are among the main factors that still hinder the commercialization of fuel cells, increasing at the same time the interest of the scientific community toward the exploration of Pt-free electrocatalysts. The last decade, a severe number of research groups world-widely have focused on the investigation of electrocatalysts with small amount or without Pt, for both the hydrogen oxidation reaction (HOR) and the oxygen reduction reaction (ORR) [3–11].

The aforementioned research and development has shot either to commonly-adopted materials, which provide enhanced Pt's utilization coefficient and consequently use of lower content of it, or to Pt-based electrocatalysts with ultra-low-Pt loading [12–14]. A great number of studies have also been devoted to the investigation of Pt combination with another metal such as Pd [15–19], Ru [20,21], Sn [2], W [2], Au [22], Mo [23], etc.

With the exception of Pt, it has been demonstrated that among pure metals, Pd exhibits relatively high electrocatalytic activity toward both HOR and ORR. This fact combined with the relatively low cost of Pd, makes it an attractive and alternative candidate for the aforementioned reactions [1,9,24–28]. However, the use of pure Pd, mostly in terms of electrocatalytic activity, has not totally and successfully replaced the role of Pt [11].

Consequently, to enhance HOR activity, various bi-metallic and tri-metallic Pd alloys such as Pd–Rh [29], Pd–Co [15,30], Pd–Au [31–33], Pd–Mo [34], Pd–Pt–Ru [17] and Pd–Pt–Rh [35] have been investigated. Nevertheless, the basic electrochemistry of Pd–Rh based electrocatalysts has not been sufficiently explored and only few reports are available in literature [29,36–38].

According to literature [24] Pd presents higher activity, than any other noble metal and comparable to that of Pt, not only for HOR but also for ORR. Active palladium-based alloys for the ORR in acid medium were presented for first time by Ota and co-workers [39,40], attracting, nevertheless, less attention than Pt due to its lower activity and stability. However, very recently, Kondo et al. [41] proved that the ORR activity of the Pd

* Corresponding author at: Department of Mechanical Engineering, School of Engineering, University of Thessaly, Pedion Areos, 38334 Volos, Greece.
Tel.: +30 24210 74065; fax: +30 24210 74050.
E-mail address: tsiak@uth.gr (P. Tsiakaras).

http://dx.doi.org/10.1016/j.apcatb.2015.03.002
0926-3373/

depends on the orientation of the index plane. More precisely, they proved that the Pd's activity toward ORR has the following order: Pd(100) » Pd(111) > Pd(110), with the Pd(100) exhibiting 14 times higher activity than Pt.

Except for the pure Pd's plane orientation, it has been shown that its activity can be enhanced by alloying it with a second or a third metal. Binary and ternary Pd – based alloys such as Pd–Ni [42–44], Pd–Cu [44,45], Pd–Fe [44], Pd–Rh [46], Pd–Ti [47], Pd–Co–Mo [48] and Pd–Co–Au [47] exhibited better electrocatalytic activity for the ORR than pure Pd and in some other cases better than that of pure Pt. Even so, PdRh bi-metallic electrocatalysts have also not been studied sufficiently for the oxygen reduction reaction.

In the present work, carbon supported (Vulcan-XC-72R) Pd_xRh_y(20 wt%) bimetallic catalysts with different atomic ratios (x:y) were prepared via a modified pulse-microwave assisted polyol method. The as-prepared electrocatalysts were physicochemically characterized using TEM and XRD techniques. Moreover, their electrocatalytic activity toward HOR and ORR was evaluated by the aid of RDE and CV methods and their stability by the chronoamperometric measurement.

2. Experimental

2.1. Electrocatalysts preparation

The examined electrocatalysts were quickly and easily prepared via a modified pulse-microwave assisted polyol synthesis. In a beaker, the starting precursors ($PdCl_2{\cdot}2H_2O$ and $RhCl_3$ provided by Strem Chemicals) were well mixed with ethylene glycol (EG) in an ultrasonic bath, and then XC-72R carbon black (Cabot Corporation) was added in the above mixture. After the adjustment of system's pH value to 13, by the drop-wise addition of 1.0 M NaOH/EG, a well dispersed slurry was obtained with ultrasonic stirring for 60 min. Thereafter, the slurry was microwave-heated in the pulse form 10 s on/10 s off for several times. In order to promote the adsorption of the suspended metal nanoparticles onto the carbon support, hydrochloric acid was adopted as the sedimentation promoter and the solution was re-acidified to a pH value of about 2–4. The resulting black solid sample was filtered, washed and dried at 80 °C for 10 h in a vacuum oven [49].

2.2. Physicochemical characterization

The X-ray diffraction (XRD) measurements were carried out by the aid of a D/Max-IIIA (Rigaku Co., Japan) employing Cu Kα (λ = 0.15406 nm) as the radiation source. The samples were scanned in the range of $10^\circ \leq 2\theta \leq 86^\circ$. Catalysts were also investigated by transmission electron microscopy (TEM) using a Philips CM12 microscope (resolution 0.2 nm), provided with high resolution camera, at an accelerating voltage of 120 kV. Suitable specimens for TEM analyses were prepared by ultrasonic dispersion in i-propylic alcohol adding a drop of the resultant suspension onto a holey carbon supported copper grid. To prevent the agglomeration of carbon supports, the prepared catalyst was diluted in ethanol using ultrasonic water bath for some minutes and dried before TEM analysis.

2.3. Electrochemical characterization

All electrochemical measurements were conducted in an electrochemical workstation AMEL 5000 adopting a saturated calomel electrode (SCE) and a Pt wire as reference and counter electrodes, respectively. Cyclic voltammetry (CV) and rotating disc electrode (RDE) measurements carried out, on a thin film catalyst deposited on a glassy carbon (GC) disc electrode (working electrode, Ø = 3.0 mm) mounted in an interchangeable RDE holder, into 0.5 M H_2SO_4 solution (Carlo Erba, 99%) at room temperature. The electrocatalytic ink was prepared by mixing 1.95 mg of electrocatalyst, 1.8 mL ethanol and 0.2 mL Nafion solution (5 wt%, IonPower, GmbH). Then, the as-prepared ink quantitatively (4 μL) was transferred onto the surface of the GC electrode and was dried to obtain a thin porous layer. For all measurements, the catalyst total loading was maintained at 11 μg cm^{-2}. Before each measurement the solution was deaerated with helium stream for 20 min. Then, hydrogen (or oxygen) gas was supplied until a saturated solution was created.

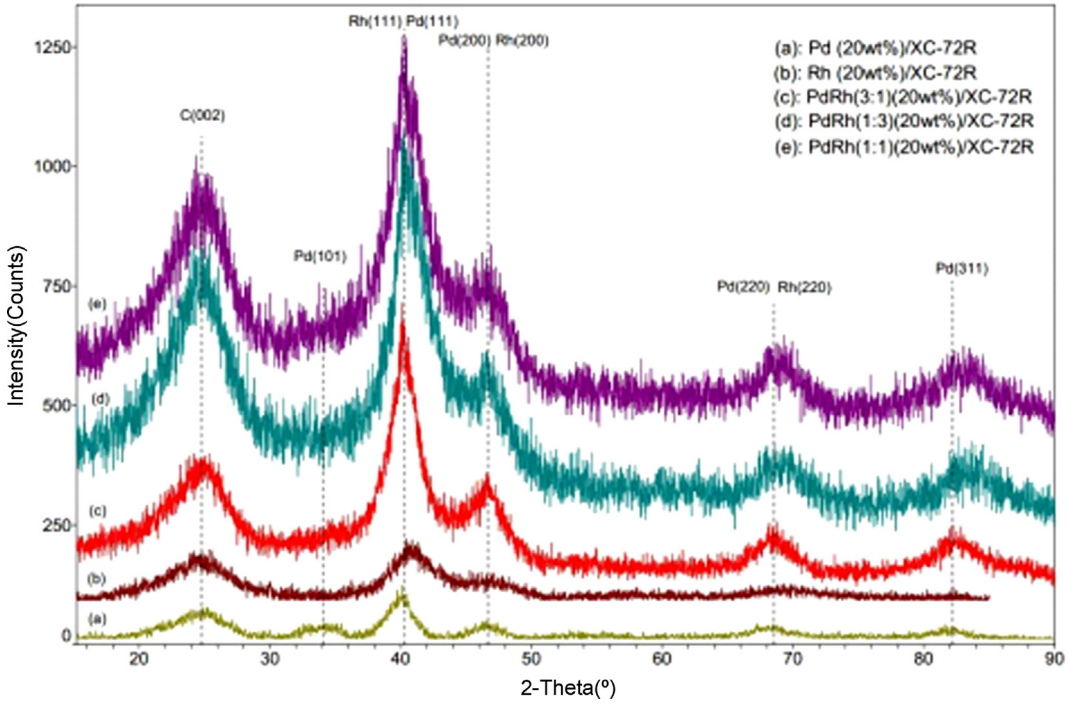

Fig. 1. X-ray diffraction patterns of (a) Pd, (b) Rh, (c) PdRh(3:1), (d) PdRh(1:3) and (e) PdRh(1:1) bimetallic catalysts prepared with polyol reduction.

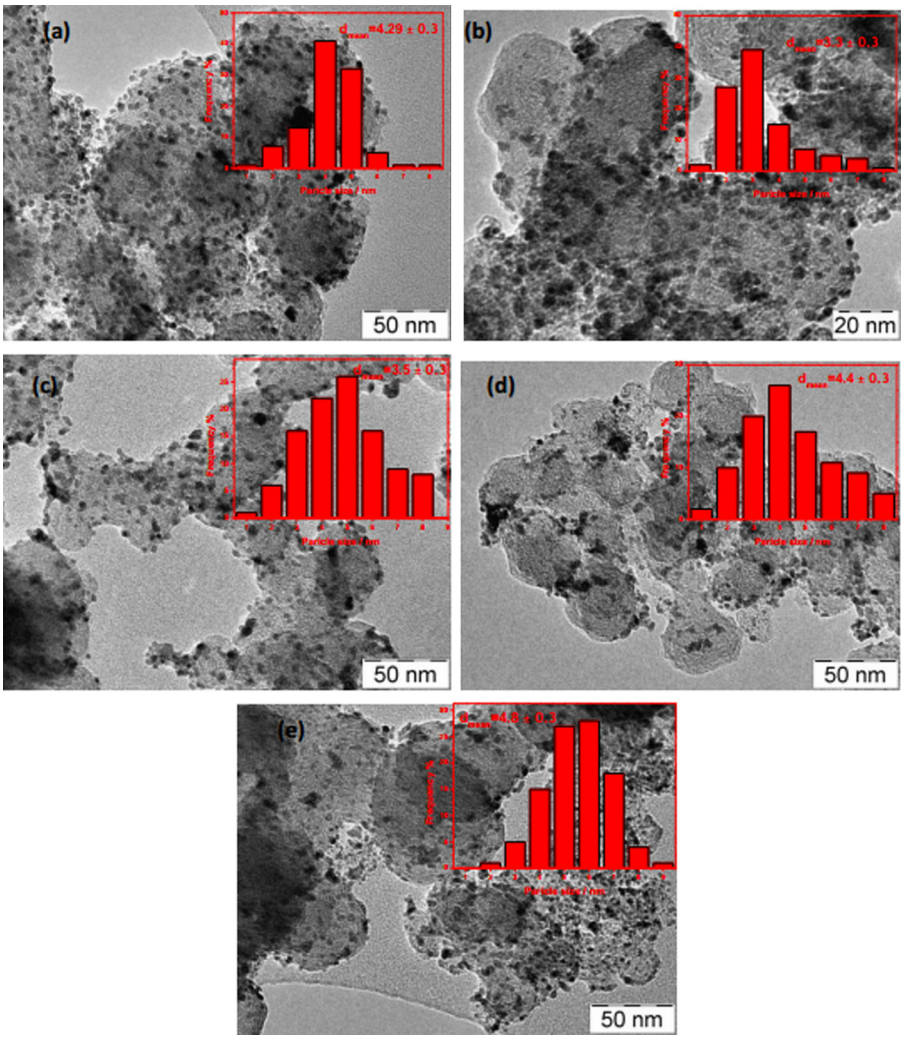

Fig. 2. TEM images of (a) Pd, (b) Rh, (c) $PdRh_3$, (d) PdRh, (e) Pd_3Rh.

During the experiments the helium (or hydrogen or oxygen) stream was directed above the solution level in order to avoid contact with air as well as keep saturated the solution (inert in case of helium). It is worth to be noticed that, for each final voltammogram several scans (reproducible) were obtained.

3. Results and discussion

3.1. Physicochemical measurements

XRD patterns of the as-prepared electrocatalysts are shown in Fig. 1.The first peak at 25° is associated with the Vulcan XC-72 support material for all the five samples. The four diffraction peaks appeared at ca. 40°, 48°, 68° and 83° belong to the face-centered cubic (fcc) crystalline Pd and Rh (1 1 1), (2 0 0), (2 2 0), (3 1 1), respectively. As it can be observed there is a peak shift toward higher 2θ values for higher Rh contents, revealing decreased lattice parameters and the high level of alloying. The (1 1 1), plane has the largest intensity among the others planes, which grows with respect to the corresponding peak of the Pd and Rh catalysts, indicating the effect of increased amounts of Rh in the Pd_xRh_y. In Table 1 the average lattice parameters and crystallite size values are reported. The above-two parameters were estimated according to Scherrer's equation [50].

As it can be seen, Pd/C has the highest lattice parameter (0.38615 nm) and crystallite size (3.0 nm), while the Rh/C the lowest one (lattice parameter: 0.38456 nm, crystallite size: 2.0 nm). The formed Pd–Rh alloys seem to present lattice parameter values between of the two pure metals, with the following order: PdRh(3:1)/C > PdRh(1:3)/C > PdRh(1:1)/C. Thus, the addition of Rh contracts the lattice parameter of Pd, decreasing also its crystallite size. This modification to the lattice parameter, may affect the hydrogen adsorption properties [35].

TEM images with the respective particle size distribution histogram of Pd/C, Rh/C and Pd_xRh_y/C catalysts are shown in Fig. 2. A remarkably uniform and high dispersion of metal particles on the carbon surface is observed concerning all the examined samples. As it can also be seen (Table 1), the mean particle size was in the following order: PdRh(3:1)/C (4.8 ± 0.3 nm) > PdRh(1:1)/C (4.4 ± 0.3 nm) > Pd/C (4.3 ± 0.3) > PdRh(1:3)/C (3.5 ± 0.3 nm) > Rh/C (3.3 ± 0.3).

Table 1
Physicochemical analysis results.

Electrode (20 wt% metal loading)	Lattice parameter (nm)	Crystallite size (nm)	Particle size (nm)
Pd/C	0.38615	3.0	4.3 ± 0.3
Rh/C	0.38456	2.0	3.3 ± 0.3
PdRh(3:1)/C	0.38794	3.0	4.8 ± 0.3
PdRh(1:1)/C	0.38474	3.5	4.4 ± 0.3
PdRh(1:3)/C	0.38516	2.0	4.3 ± 0.3

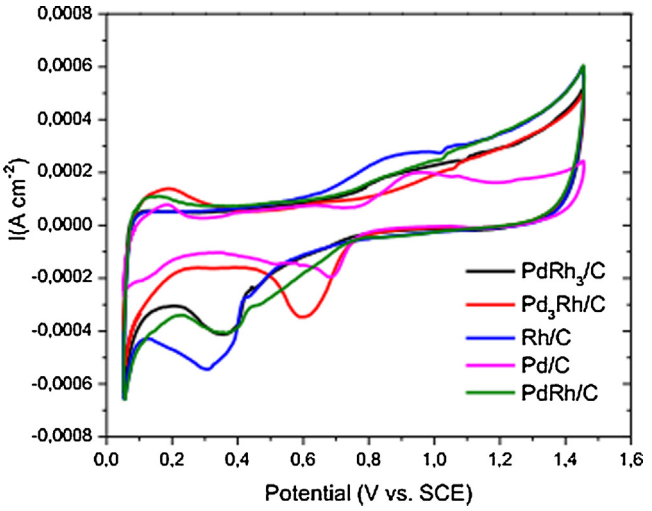

Fig. 3. Cyclic voltammograms for (a) Pd, (b) Pd_3Rh, (c) PdRh and (d) $PdRh_3$ in 0.5 M H_2SO_4, scan rate: 50 mV s^{-1}.

Table 2
Cyclic voltammetry analysis.

Electrode (20 wt% metal loading)	Pd loading ($\mu g\,cm^{-2}$)	Rh loading ($\mu g\,cm^{-2}$)	ECSA ($m^2\,g^{-1}_{metal}$)
Pd/C	11	0	21.0
PdRh(3:1)/C	8.3	2.7	22.5
PdRh(1:1)/C	5.6	5.4	27.0
PdRh(1:3)/C	2.8	8.2	29.5
Rh/C	0	11	25.6

3.2. Electrochemical catalytic surface area

The voltammetric profiles recorded for Pd, Rh, and Pd_xRh_y alloys obtained in 0.5 M H_2SO_4 solution and with a scan rate of 50 mV s^{-1}, are schematically shown in Fig. 3. The electrochemical active surface area (ECSA) was estimated by the aid of the following equation [51], taking into account the reduction peak that is observed during the backward scanning:

$$\mathrm{ECSA}\left[\frac{m^2}{g}\right] = \frac{Q_H}{(Q_{PdorRh}) \times m_{PdorRh} \times 10}$$

where $Q_H = (Q_{ads} + Q_{des})/2$ ($\mu C\,cm^{-2}{}_{Pt}$) represents the average charge extracted from the integration of the adsorption/desorption hydrogen regions of the CV curves, $Q_{Pd} = 420\,\mu C\,cm^{-2}{}_{Pd}$ and $Q_{Rh} = 256\,\mu C\,cm^{-2}{}_{Rh}$ [52] are the specific amount of electricity corresponding to the full coverage of the Pd or Rh surface by one monolayer of oxygen and $m_{Pd(Rh)}$ ($mg\,cm^{-2}{}_{electrode}$) is the palladium or rhodium loading on the working electrode's surface. The results of the ECSA calculations, for the electrocatalysts used in the present investigation are reported in Table 2. As it can be noticed, the electrochemical active surface area exhibits the following order: Pd/C < Pd_3Rh/C < Rh/C < PdRh/C < $PdRh_3$/C.

3.3. Hydrogen oxidation reaction kinetics

The HOR polarization curves for the Pd/C, Rh/C and Pd_xRh_y/C electrocatalysts are depicted in Fig. 4. As it can be distinguished, the oxidation of H_2 over the Pd_xRh_y/C alloys and pure Rh/C starts at potential values around to 0.01 V (onset potential), while over pure Pd/C electrocatalyst the HOR's onset potential is higher, ca 0.1 V. It can also be seen that, the current continues increasing sharply up to 0.1 V and 0.2 V for the Pd_xRh_y/C, Rh/C and pure Pd/C, respectively. At more positive potentials, transition into the region of hydrogen mass transport controlled current densities starts at approximately 0.15 V. As it was expected, the limiting current increases with the increment of the rotational speed of the electrode [53]. Moreover, the electrochemical behavior of the as prepared Pd_xRh_y electrocatalysts is similar to that of pure Rh. As it is well known, during a reaction the kinetic current density (i_k) is a measure of the rate of charge transfer on the catalyst's surface.

Table 3
Kinetic analysis results for hydrogen oxidation reaction.

Electrode (20 wt% metal loading)	Tafel slope (mV $decade^{-1}$)	i_o(mA cm^{-2})	i_k(@0.1 V) (mA cm^{-2})
Pd/C	80.0	0.32	3.0
PdRh(3:1)/C	120.0	1.24	4.0
PdRh(1:1)/C	230.0	2.56	7.3
PdRh(1:3)/C	180.0	3.00	7.6
Rh/C	210.0	2.58	6.0

More precisely, i_k describes the real kinetics of an electrocatalytic reaction and therefore, is directly related to the activity of an electrocatalyst. To determine the catalytic activity of the electrocatalysts, we adopted the Koutecky–Levich analysis [54], where the kinetic current is related to the rotational velocity of the RDE through the following equation:

$$\frac{1}{i} = \frac{1}{i_k} + \frac{1}{i_d} \quad (1)$$

where i represents the experimental value of the current, i_k the kinetic current in the absence of mass transfer limitations and i_d the diffusion-limited current. The later can be calculated according to the Levich equation:

$$i_d = 0.62nFD^{2/3}\nu^{-1/6}C\omega^{1/2} \quad (2)$$

where n is the number of theoretically-transferred electrons (=2), F the Faraday constant (95,485 C/mol), D the diffusion coefficient of H_2 in the H_2SO_4, ν the kinematic viscosity of the electrolyte and C the H_2 concentration in the electrolyte. The kinetic current density was graphically determined ($1/i$ vs. $1/\omega^{1/2}$ – Koutecky–Levich plots).

The insets of Fig. 4 provide the Koutecky–Levich plots for the examined Pd_xRh_y/C, Pd/C and Rh/C electrocatalysts, from which the kinetic currents for HOR, at 0.1 V (vs. SCE), were extracted. As follows from their analysis, the experimental points have a linear behavior ensuring the accuracy of i_k determination.

The kinetic current density values were calculated to be 6.0, 7.6, 7.3, 4.0 and 3.0 mA cm^{-2} for Rh, $PdRh_3$, PdRh, Pd_3Rh and Pd, respectively. It is obvious that among the as prepared electrocatalysts, PdRh and $PdRh_3$ exhibit the highest electrocatalytic activity toward hydrogen electrooxidation and comparable to that of Pt's, as reported in literature (Fig. 6) [55,56]. After that, the kinetic analysis the Tafel–Heyrovsky (mass-transfer corrected) plots were also obtained (Fig. 5) after the measured currents were corrected for diffusion to obtain the kinetic current [57].

$$\log(i_k) = \log(i_o) + \left(\frac{anF}{2.303RT}\right)\eta \quad (3)$$

where $i_k = \frac{i \times i_d}{i_d - i}$, as being calculated from the Koutecky–Levich plots.

The slope of Tafel plots ($\partial \log jk/\partial E$), varies with the electrode potential, lacking an extended linear Tafel region. It is well known that, from the Tafel slope and intercept useful kinetic information can be obtained [58]: (i) the exchange current density and (ii) the charge transfer coefficient. From the kinetic analysis (Table 3) it is deduced that $PdRh_3$'s activity predominates over other electrocatalysts, followed by the PdRh and Rh. Moreover, from the slope values and in accordance with the literature, the hydrogen oxidation reaction on the as prepared samples, follows the

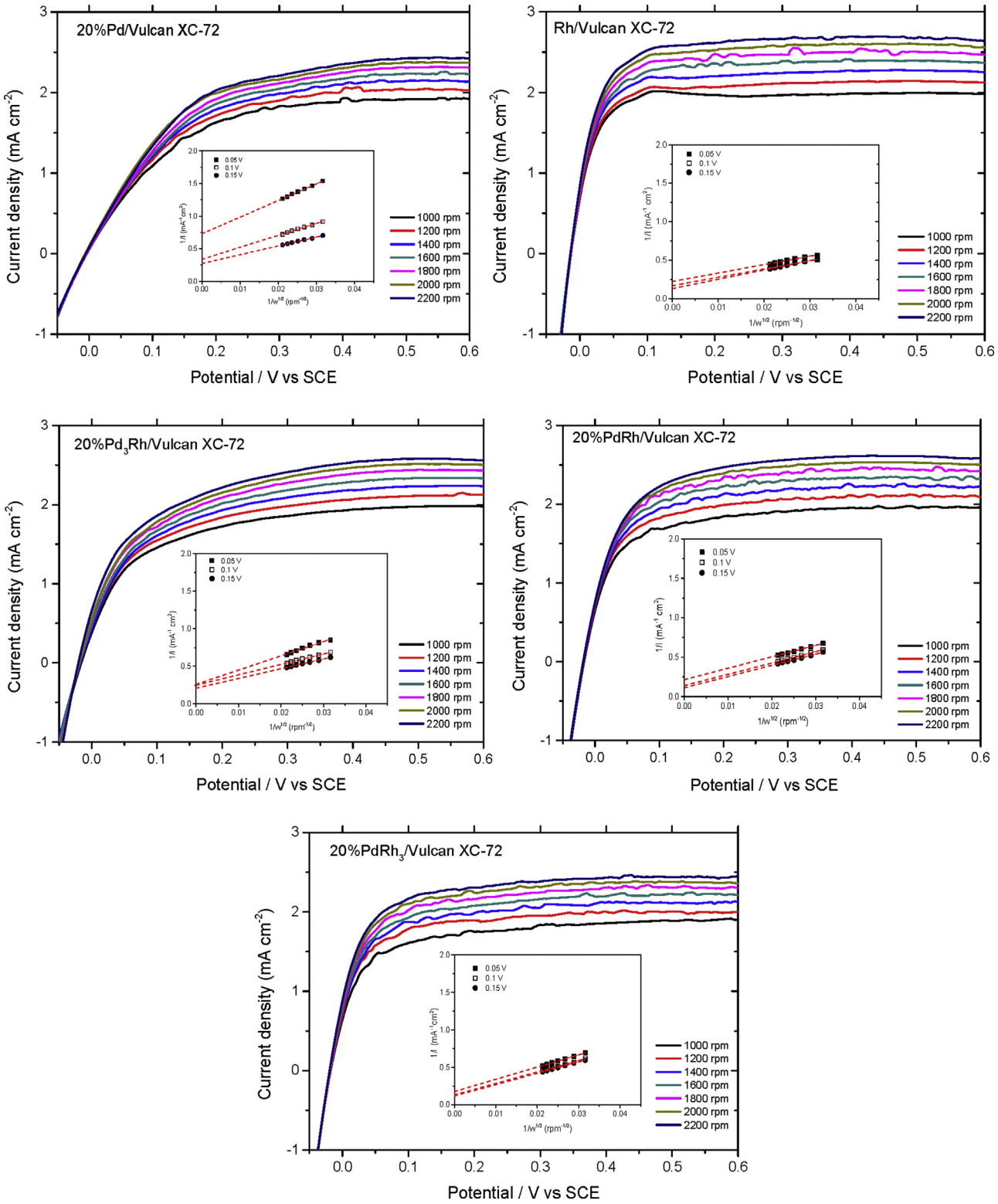

Fig. 4. RDE curves in H_2-saturated 0.5 M H_2SO_4, scan rate: 5 mV s^{-1}. Insets: Koutecky–Levich plots. The insets are the corresponding Koutecky–Levich plots for the hydrogen oxidation reaction.

Tafel–Heyrovsky–Volmer mechanism, as with Pt-based electrocatalysts do [24]. Furthermore the exchange current density value measured for Pd is quite close to those reported in literature, 0.29 mA cm^{-2} by Shao [24] and 0.22 mA cm^{-2} by Pronkin et al. [59].

Additionally, from the values of the charge transfer coefficient (α), which all were calculated to be close to 0.25, maybe due to the increased overpotential [60]. The charge transfer coefficient represents the fraction of additional energy that goes toward the reaction at the electrode. Also the mass corrected Tafel slopes are calculated and reported in Table 3. According to literature [61–63] and the reported slopes the adsorption dissociation of hydrogen on the catalyst surface is the rate determining step (Volmer), taking into consideration the Tafel–Heyrovsky–Volmer mechanism for HOR:

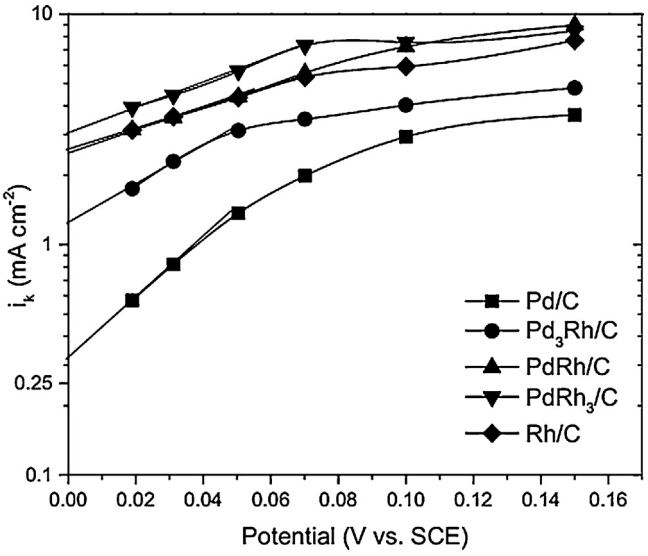

Fig. 5. Tafel plots for HOR.

$H_2 \rightleftharpoons 2H_{ad}$: Tafel
$H_2 \rightleftharpoons H_{ad} + e^- + H^+$: Heyrovsky
$H_{ad} \rightleftharpoons H^+ + e^-$: Volmer

In order to obtain a more thorough understanding about the effect of Rh loading to the activity (to the kinetic and exchange current) of the examined electrocatalysts, Fig. 7 is given. From this it can be deduced that, the increase of the Rh loading strongly enhances the electrocatalytic activity of Pd toward HOR in terms of both exchange current and kinetic density. The increased electrocatalytic activity of PdRh bimetallic electrocatalysts could be attributed to their ability to adsorb more hydrogen than pure Pd, as it has been declared by Żurowski et al. [64]. On the other hand, according to Zum Mallen et al. [65], the higher (than pure Pd) electrocatalytic activity was measured for pure Rh/C, could be attributed to the fact that Rh, has the same hydrogen binding energy with Pt.

3.4. Chronoamperometric measurements

The stability of the examined electrocatalysts for hydrogen electro oxidation in 0.5 M H_2SO_4 at 25 °C for 1300 s was investigated by chronoamperometric measurements, and the results are reported

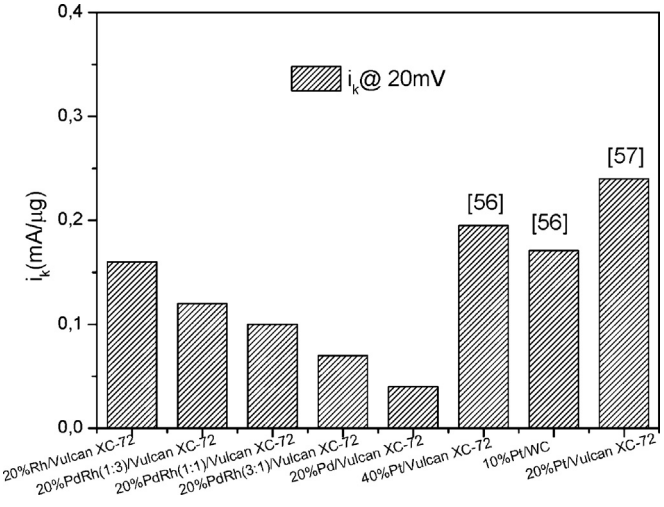

Fig. 6. Comparison of kinetic current density for HOR.

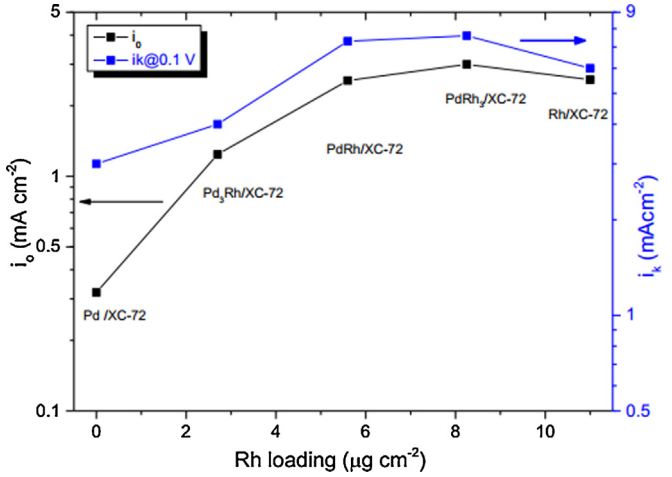

Fig. 7. Exchange current density and kinetic current density vs. rhodium metal loading for HOR.

in Fig. 8. As can be seen in Fig. 8 the $PdRh_3$/Vulcan XC-72 catalyst appears to have the same current decay with PdRh after 200 s, however, after 200 s $PdRh_3$ show better long term stability. That means that the addition of rhodium hinders pure palladium from leaching, giving higher stability to Pd's electrocatalyst. Furthermore the chronoamperometric measurements further confirmed pure Rh's, PdRh and $PdRh_3$ enhanced catalytic activity toward hydrogen oxidation reaction.

3.5. Oxygen reduction reaction kinetics

The tests for ORR activity of the electrocatalysts were conducted in oxygen-saturated 0.5 M H_2SO_4 solution, from 0 to 0.90 V (vs. SCE), at different rotation rates (from 500 to 2500 rpm) and at constant sweep rate of 10 mV s^{-1}.

As it is schematically shown in Fig. 9, well-defined limiting currents were observed increasing the rotation rate due to the increased availability of oxygen at the electrodes surface. In each polarization curve three different characteristic regions are displayed: The first region which is observed from 0.9 to 0.65 V (vs. SCE) is the kinetic one, where the kinetic current is independent of the rotation rate. The second one is the mixed control region and it is observed from 0.65 to 0.2 V (vs. SCE). In this, the current is controlled by both kinetic as well as diffusion-limited processes. Finally

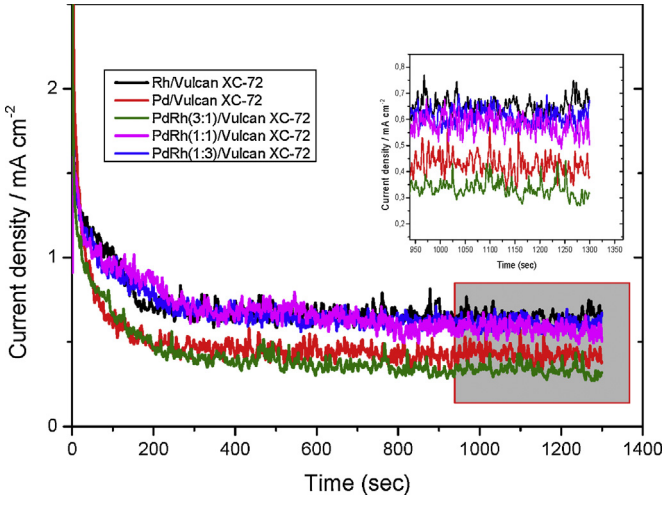

Fig. 8. Chronoamperometry curves for HOR, in 0.5 M H_2SO_4 for 1300 s at 0.25 V.

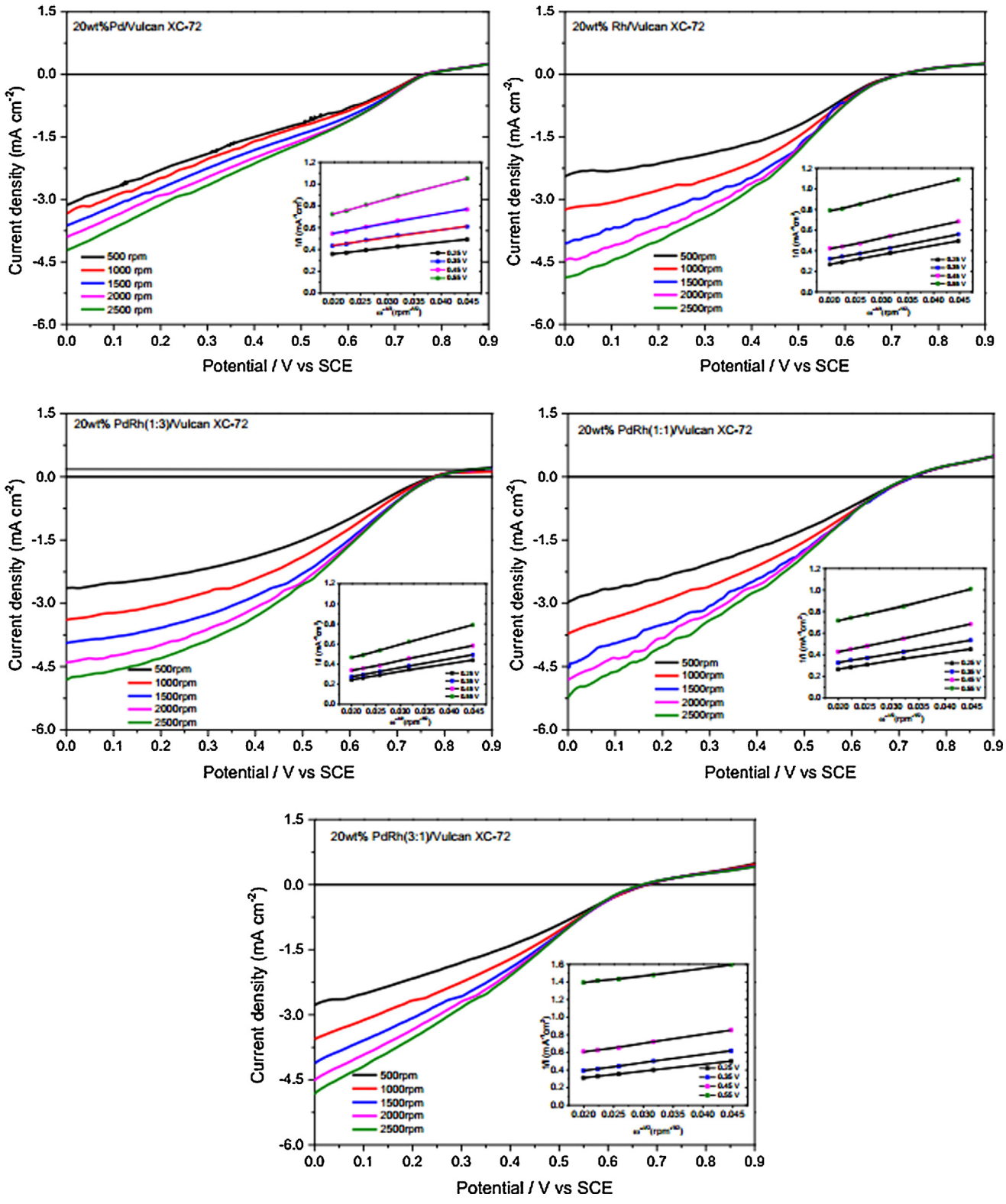

Fig. 9. RDE curves of (A) Pd, (B) Rh, (C) $PdRh_3$, (D) PdRh and (E) Pd_3Rh electrodes in O_2-saturated 0.5 M H_2SO_4, scan rate: 10 mV s^{-1}.

in the third region, from 0.2 to 0.0 V (vs. SCE) the ORR curve is under mass transport control limited by the diffusion of the dissolved oxygen in the electrolyte [66]. In the last region the polarization curves do not catch a flat plateau; behavior that can be explained from irreversible electrode processes [67]. Another possible explanation is that the film that was formed on the working electrode was very thin, due to the low amount of catalytic ink (4 μL) that was deposited on it in order to have very low catalyst loading. The onset potential for all the examined samples is observed to be the same, ca 0.7 V (vs. SCE) and the limiting diffusion currents 4.15, 4.70, 4.79, 4.80 and 4.86 mA cm^{-2} (at 2500 rpm) for the Pd, Pd_3Rh, PdRh, $PdRh_3$ and Rh, respectively.

Koutecky–Levich equation (Eq. (1)) was adopted to determine the kinetic parameters of the electrocatalysts: (i) the kinetic current

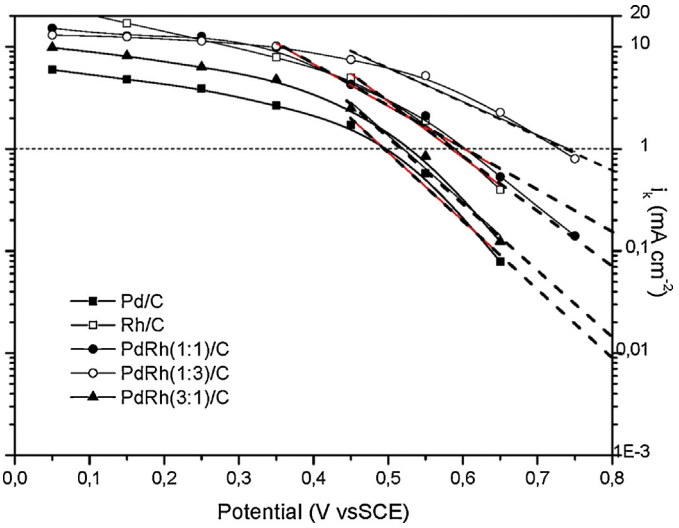

Fig. 10. Tafel plots for ORR.

density and (ii) the number of electrons that take part into the reaction. More precisely, from the intercept of Koutecky–Levich plots (insets of Fig. 9) and using Levich equation:

$$i_d = 0.62nFD^{2/3}\nu^{-1/6}C\omega^{1/2} \quad (4)$$

where n is the number of electrons involved in the reaction, F is the Faraday constant (96,485 C/mol), D is the diffusion coefficient of O_2 in the H_2SO_4 (1.4×10^{-5} cm^2 s^{-1}), ν is the kinematic viscosity of the electrolyte (1.0×10^{-2} cm^{-2} s^{-1}), C is the O_2 concentration in the electrolyte (1.1×10^{-6} mol cm^{-3}), are calculated the kinetic current density values and from the slope, the total number of electrons involved in the reaction [68]. Then for further kinetic analysis the Tafel plots (Fig. 10) were done, from which: (i) the exchange current density and (ii) Tafel slopes and charge transfer coefficients, are also calculated.

The linearity and parallelism of the Koutecky–Levich plots show the first-order kinetics with respect to molecular oxygen (insets of Fig. 9). The kinetic current density is proportional to the intrinsic activity of the catalysts and the slopes of the straight lines allow us to estimate the number of electrons involved in the ORR [69]. Except for Pd where the total electrons involved in the reaction are two, for all the others examined electrocatalysts the total electrons are four.

A widely accepted method to determine the ORR activity of an electrocatalyst is based on the half-wave potential, which is defined as the potential at which the magnitude of the current is half of the limiting current [66].

According to theory [70], ORR in aqueous solution occurs mainly following two pathways: the direct 4-electron reduction pathway from O_2 to H_2O, and the 2-electron reduction pathway from O_2 to hydrogen peroxide (H_2O_2). In the present case and from the kinetic analysis for all the examined electrocatalysts the total electrons that are transferred during the oxygen reduction reaction are four.From Fig. 11 it can be deduced that, the addition of the Rh loading to Pd also enhances the electrocatalytic activity of Pd toward ORR in terms of both exchange current and kinetic density. The kinetic current density at half-wave potential (0.55 V) is higher for the $PdRh_3$ (5.20 mA cm^{-2}), followed by PdRh and Pd (2.10 mA cm^{-2}) and by pure Rh (1.89 mA cm^{-2}) and finally by the Pd_3Rh (0.89 mA cm^{-2}). The addition of specific amount of Rh (>5.4 μg cm^{-2}) to pure Pd increases the kinetic current density by 147%. As it is expected pure palladium and high palladium loading (Pd_3Rh) do not enhance the oxygen reduction reaction in comparison with the other electrocatalysts (Rh, PdRh and $PdRh_3$). This is

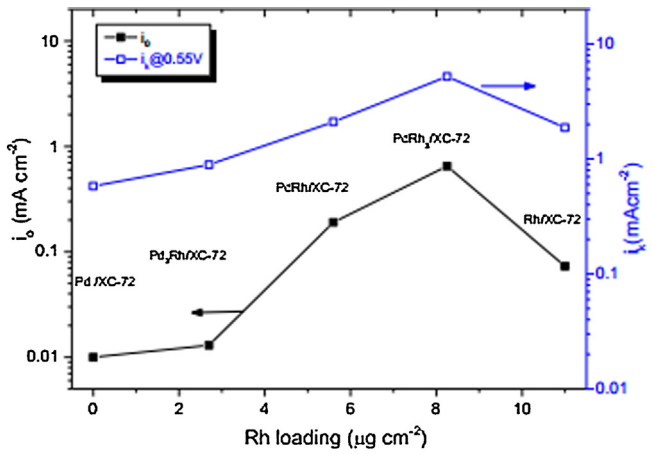

Fig. 11. Exchange current density and kinetic current density vs. rhodium metal loading for ORR.

Table 4
Kinetic analysis results for oxygen reduction reaction.

Electrode (20 wt% metal loading)	Tafel slope (mV decade^{-1})	i_o(mA cm^{-2})	i_k(@0.55 V) (mA cm^{-2})
Pd/C	131	0.01	0.58
PdRh(3:1)/C	140	0.015	0.89
PdRh(1:1)/C	149	0.18	2.10
PdRh(1:3)/C	110	0.65	5.20
Rh/C	111	0.08	1.87

also confirmed by their low reaction rate constant (Table 4). Additionally, the obtained Tafel slopes were calculated at a range of ~200 mV and are reported in Table 4.

As it is well known from the theory, for $T = 298$ K, $\alpha = 0.5$ and $n = 1$or 2, two slopes have been should be reported: 120 mV/decade ($n = 1$) and 60 mV decade^{-1} ($n = 2$). From the calculated Tafel slopes (slope = 2.303RT/αFn) the electrons involved in the rate determining step can be estimated [68].

It should be noted that, in the current work, the estimated Tafel slopes (Table 4) are very high (in comparison with the value of 120 mV decade^{-1}), due to the high overpotential. The high overpotential may attributed to mass transport phenomena [71].

4. Conclusions

From the analysis of the obtained results the following conclusions can be drawn:

Pd-based electrocatalysts could play a great role to whole or partially replace costly Pt in both anode and cathode compartments, at low temperature H_2-PEMFCs.

Pure Rh and Pd–Rh binary alloys show comparable or higher hydrogen oxidation and oxygen reduction activity than pure Pd.

The HOR activity order, in terms of kinetic current density, is the following: $PdRh_3$ (7.6 mA cm^{-2}) > PdRh (7.3 mA cm^{-2}) > Rh (6.0 mA cm^{-2}) > Pd_3Rh (4.0 mA cm^{-2}) > Pd (3.0 mA cm^{-2}). Rhodium's enhanced activity toward HOR may be attributed to its high (as Pt's) hydrogen binding energy. However, the higher (than pure Pd) palladium–rhodium bimetallic electrocatalysts' activity is probably due to their ability to adsorb more hydrogen.

According to the chronoamperometric results, the addition of rhodium also increases the stability of pure palladium, since it hinders the last from leaching, due to the corrosive environment of the acidic medium. As the kinetic analysis shown, over all the samples the hydrogen oxidation reaction was charge transfer controlled. The ORR activity order at half wave potential, in terms of kinetic current density, is the following: $PdRh_3$ (5.2 mA cm^{-2}) > PdRh ≈ Pd

($2.10\,mA\,cm^{-2}$) > Rh ($1.89\,mA\,cm^{-2}$) > Pd_3Rh ($0.89\,mA\,cm^{-2}$). Consequently, also the addition of a certain amount of rhodium ($8.2\,\mu g cm^{-2}$) significantly enhances the activity of pure palladium. According to the kinetic analysis, all the examined electrocatalysts seem to follow the two-way pathway with four electrons total to be included in the oxygen reduction reaction process.

Summarizing, the addition even of small amounts of Rh ($2.7\,\mu g_{Rh}\,cm^{-2}$) as a second metal to Pd (24.5%Rh) contributes to the activity increment toward both the hydrogen oxidation and oxygen reduction reaction by 132% and 80%, respectively.

Finally, according to the as-reported results, also pure Rh could be a possible alternative for higher anodic and cathodic catalytic activity, however it's very high cost do not make it appealing for further investigation.

Acknowledgments

Dr F. Tzorbatzoglou, is grateful to the Research Funding Program: Heracleitus II which is co-financed by the European Union (European Social Fund – ESF) and Greek National Funds through the Operational Program "Education and Lifelong Learning" of the National Strategic Reference Framework (NSRF, 2007–2013)-investing in knowledge society through the European Social Fund. Moreover, Prof. P. Tsiakaras and Dr A. Brouzgou are grateful to the Ministry of Education and Science of the Russian Federation (contract no. 14.Z50.31.0001) and to "Bilateral R&D Co-operation between Greece and China 2012–2014", co-financed by the European Union and the Greek Ministry of Education-GSRT, for financial support.

References

[1] S. Trasatti, J. Electroanal. Chem. 39 (1972) 163–184.
[2] M. Götz, H. Wendt, Electrochim. Acta 43 (1998) 3637–3644.
[3] W. Vielstich, A. Lamm, H.A. Gasteiger, Handbook of Fuel Cells: Fundamentals, Technology, Applications, 4-Volume Set 2003.
[4] Holladay, J. Hu, D.L. King, Y. Wang, Catal. Today 139 (2009) 244–260.
[5] H.A. Gasteiger, S.S. Kocha, B. Sompalli, F.T. Wagner, Appl. Catal. B: Environ. 56 (2005) 9–35.
[6] X. Liu, E.H. Yu, K. Scott, Appl. Catal. B: Environ. 162 (2015) 593–601.
[7] C. Domínguez, F.J. Pérez-Alonso, M. Abdel Salam, S.A. Al-Thabaiti, A.Y. Obaid, A.A. Alshehri, J.L. Gómez de la Fuente, J.L.G. Fierro, S. Rojas, Appl. Catal. B: Environ. 162 (2015) 420–429.
[8] S.N. Stamatin, M. Borghei, R. Dhiman, S.M. Andersen, V. Ruiz, E. Kauppinen, E.M. Skou, Appl. Catal. B: Environ. 162 (2015) 289–299.
[9] E. Antolini, Energy Environ. Sci. 2 (2009) 915–931.
[10] B. Li, Z. Yan, D.C. Higgins, D. Yang, Z. Chen, J. Ma, J. Power Sources 262 (2014) 488–493.
[11] K. Kwon, S.-A. Jin, K.H. Lee, D.J. You, C. Pak, Catal. Today 232 (2014) 175–178.
[12] S. Vengatesan, H.J. Kim, S.K. Kim, I.H. Oh, S.Y. Lee, E. Cho, H.Y. Ha, T.H. Lim, Electrochim. Acta 54 (2008) 856–861.
[13] D. Dang, S. Liao, F. Luo, S. Hou, H. Song, P. Huang, J. Power Sources 260 (2014) 27–33.
[14] A. Brouzgou, S.Q. Song, P. Tsiakaras, Appl. Catal. B: Environ. 127 (2012) 371–388.
[15] F. Kadirgan, A.M. Kannan, T. Atilan, S. Beyhan, S.S. Ozenler, S. Suzer, A. Yörür, Int. J. Hydrogen Energy 34 (2009) 9450–9460.
[16] Y.H. Cho, B. Choi, H.S. Park, Y.E. Sung, Electrochem. Commun. 9 (2007) 378–381.
[17] A.C. Garcia, V.A. Paganin, E.A. Ticianelli, Electrochim. Acta 53 (2008) 4309–4315.
[18] S.J. Yoo, H.-Y. Park, T.-Y. Jeon, I.-S. Park, Y.-H. Cho, Y.-E. Sung, Angew. Chem. Int. Ed. 47 (2008) 9307–9310.
[19] D.C. Papageorgopoulos, M. Keijzer, J.B.J. Veldhuis, F.A. De Bruijn, J. Electrochem. Soc. 149 (2002) A1400–A1404.
[20] T. Yamanaka, T. Takeguchi, G. Wang, E.N. Muhamad, W. Ueda, J. Power Sources 195 (2010) 6398–6404.
[21] W.C. Chang, M.T. Nguyen, J. Power Sources 196 (2011) 5811–5816.
[22] R. Zeis, A. Mathur, G. Fritz, J. Lee, J. Erlebacher, J. Power Sources 165 (2007) 65–72.
[23] T. Ioroi, N. Fujiwara, Z. Siroma, K. Yasuda, Y. Miyazaki, Electrochem. Commun. 4 (2002) 442–446.
[24] M. Shao, J. Power Sources 196 (2011) 2433–2444.
[25] P.S. Ruvinsky, S.N. Pronkin, V.I. Zaikovskii, P. Bernhardt, E.R. Savinova, Phys. Chem. Chem. Phys. 10 (2008) 6665–6676.
[26] J. Moreira, P. del Angel, A.L. Ocampo, P.J. Sebastián, J.A. Montoya, R.H. Castellanos, Int. J. Hydrogen Energy 29 (2004) 915–920.
[27] C. Gabrielli, P.P. Grand, A. Lasia, H. Perrot, J. Electrochem. Soc. 151 (2004) A1937–A1942.
[28] M.S. Rau, P.M. Quaino, M.R. Gennero de Chialvo, A.C. Chialvo, Electrochem. Commun. 10 (2008) 208–212.
[29] M. Łukaszewski, A. Czerwiński, J. Alloys Compd. 473 (2009) 220–226.
[30] V. Di Noto, E. Negro, S. Lavina, S. Gross, G. Pace, Electrochim. Acta 53 (2007) 1604–1617.
[31] N.A. Maiorova, A.A. Mikhailova, O.A. Khazova, V.A. Grinberg, Russ. J. Electrochem. 42 (2006) 331–338.
[32] T.J. Schmidt, Z. Jusys, H.A. Gasteiger, R.J. Behm, U. Endruschat, H. Boennemann, J. Electroanal. Chem. 501 (2001) 132–140.
[33] M. Łukaszewski, K. Kuśmierczyk, J. Kotowski, H. Siwek, A. Czerwiński, J. Solid State Electrochem. 7 (2003) 69–76.
[34] M. Ura, Y. Haraguchi, F.L. Chen, Y. Sakamoto, J. Alloys Compd. 231 (1995) 436–439.
[35] M. Łukaszewski, M. Grdeń, A. Czerwiński, J. Electroanal. Chem. 573 (2004) 87–98.
[36] M.A. Montero, J.L. Fernández, M.R. Gennero de Chialvo, A.C. Chialvo, J. Power Sources 254 (2014) 218–223.
[37] A. Czerwinski, M. Lukaszewski, A. Zurowski, H. Siwek, S. Obrebowski, J. New Mater. Electrochem. Syst. 9 (2006) 419–429.
[38] M. Łukaszewski, A. Czerwiński, J. Solid State Electrochem. 11 (2007) 339–349.
[39] O. Savadogo, K. Lee, S. Mitsushima, N. Kamiya, K.I. Ota, J. New Mater. Electrochem. Syst. 7 (2004) 77–83.
[40] O. Savadogo, K. Lee, K. Oishi, S. Mitsushima, N. Kamiya, K.I. Ota, Electrochem. Commun. 6 (2004) 105–109.
[41] S. Kondo, M. Nakamura, N. Maki, N. Hoshi, J. Phys. Chem. C 113 (2009) 12625–12628.
[42] J. Zhao, A. Sarkar, A. Manthiram, Electrochim. Acta 55 (2010) 1756–1765.
[43] G. Ramos-Sánchez, H. Yee-Madeira, O. Solorza-Feria, Int. J. Hydrogen Energy 33 (2008) 3596–3600.
[44] X. Wang, N.N. Kariuki, S. Niyogi, M.C. Smith, D.J. Myers, T. Hofmann, Y. Zhang, M. Bär, C. Heske, ECS Trans. 2 PART (1 ed) (2008) 109–119.
[45] X. Wang, N. Kariuki, J.T. Vaughey, J. Goodpaster, R. Kumar, D.J. Myers, J. Electrochem. Soc. 155 (2008) B602–B609.
[46] Y. Qi, J. Wu, H. Zhang, Y. Jiang, C. Jin, M. Fu, H. Yang, D. Yang, Nanoscale 6 (2014) 7012–7018.
[47] J.L. Fernández, V. Raghuveer, A. Manthiram, A.J. Bard, J. Am. Chem. Soc. 127 (2005) 13100–13101.
[48] V. Raghuveer, A. Manthiram, A.J. Bard, J. Phys. Chem. B 109 (2005) 22909–22912.
[49] S. Song, J. Liu, J. Shi, H. Liu, V. Maragou, Y. Wang, P. Tsiakaras, Appl. Catal. B: Environ. 103 (2011) 287–293.
[50] A.L. Patterson, Phys. Rev. 56 (1939) 978–982.
[51] D. Chi Linh, P. Thy San, N. Ngoc Phong, T. Viet Quan, Adv. Nat. Sci.: Nanosci. Nanotechnol. 4 (2013) 035011.
[52] T. Langkau, H. Baltruschat, Electrochim. Acta 44 (1998) 909–918.
[53] R. Escudero-Cid, A.S. Varela, P. Hernández-Fernández, E. Fatás, P. Ocón, Int. J. Hydrogen Energy 39 (2014) 5063–5073.
[54] J. Durst, A. Siebel, C. Simon, F. Hasche, J. Herranz, H.A. Gasteiger, Energy Environ. Sci. 7 (2014) 2255–2260.
[55] V.M. Nikolic, D.L. Zugic, I.M. Perovic, A.B. Saponjic, B.M. Babic, I.A. Pasti, M.P. Marceta Kaninski, Int. J. Hydrogen Energy 38 (2013) 11340–11345.
[56] A.B. Suryamas, G.M. Anilkumar, S. Sago, T. Ogi, K. Okuyama, Catal. Commun. 33 (2013) 11–14.
[57] S.J. Yoo, H.-Y. Park, T.-Y. Jeon, I.-S. Park, Y.-H. Cho, Y.-E. Sung, Angew. Chem. 120 (2008) 9447–9450.
[58] D.L. Langhus, J. Chem. Educ. 76 (1999) 1069.
[59] S.N. Pronkin, A. Bonnefont, P.S. Ruvinskiy, E.R. Savinova, Electrochim. Acta 55 (2010) 3312–3323.
[60] S.T. Revankar, P. Majumdar, Fuel Cells: Principles, Design, and Analysis, Taylor & Francis, 2014, 2015.
[61] W. Sheng, H.A. Gasteiger, Y. Shao-Horn, J. Electrochem. Soc. 157 (2010) B1529–B1536.
[62] D. Pletcher, Royal Society of Chemistry, A First Course in Electrode Processes, Royal Society of Chemistry, Cambridge, UK, 2009.
[63] T.J. Schmidt, V. Stamenkovic, N.M. Markovic, P.N. Ross Jr., Electrochim. Acta 48 (2003) 3823–3828.
[64] A. Żurowski, M. Łukaszewski, A. Czerwiński, Electrochim. Acta 51 (2006) 3112–3117.
[65] M.P. Zum Mallen, W.R. Williams, L.D. Schmidt, J. Phys. Chem. 97 (1993) 625–632.
[66] Y. Sun, Y.-C. Hsieh, L.-C. Chang, P.-W. Wu, J.-F. Lee, J. Power Sources 277 (2015) 116–123.
[67] R.H. Castellanos, A.L. Ocampo, P.J. Sebastian, J. New Mater. Electrochem. Syst. 5 (2002) 83–90.
[68] W. Xing, G. Yin, J. Zhang, Rotating Electrode Methods and Oxygen Reduction Electrocatalysts, Elsevier Science, 2014.
[69] J.J. Salvador-Pascual, S. Citalán-Cigarroa, O. Solorza-Feria, J. Power Sources 172 (2007) 229–234.
[70] J. Zhang, PEM Fuel Cell Electrocatalysts and Catalyst Layers: Fundamentals and Applications, Springer, 2008.
[71] S.L. Gojković, S. Gupta, R.F. Savinell, J. Electroanal. Chem. 462 (1999) 63–72.